Imaging beyond the ballistic limit in coherence imaging using multiply scattered light

Michael G. Giacomelli[1] and Adam Wax[1,*]

[1]*Department of Biomedical Engineering and Fitzpatrick Center for Photonics, Duke University, Durham, North Carolina 27708, USA*
**a.wax@duke.edu*

Abstract: We present an imaging system based on low coherence interferometric detection of multiply scattered light for extended depth imaging into highly scattering media. By incorporating angle-resolved detection, coherence imaging with multiply scattered photons is shown to be both feasible and potentially superior to existing techniques for performing time-resolved measurements of scattered light. Imaging is demonstrated through nearly 100 mean free paths of scattering phantom in a single-ended geometry. The resolution and imaging contrast are compared to those obtained with conventional OCT systems which chiefly detect singly scattered light.

OCIS codes: (290.0290) Scattering; (100.3175) Interferometric imaging; (290.4210) Multiple scattering.

References and links

1. J. A. Izatt, M. R. Hee, G. M. Owen, E. A. Swanson, and J. G. Fujimoto, "Optical coherence microscopy in scattering media," Opt. Lett. **19**(8), 590–592 (1994).
2. M. A. Choma, M. V. Sarunic, C. H. Yang, and J. A. Izatt, "Sensitivity advantage of swept source and Fourier domain optical coherence tomography," Opt. Express **11**(18), 2183–2189 (2003).
3. M. R. Hee, J. A. Izatt, J. M. Jacobson, J. G. Fujimoto, and E. A. Swanson, "Femtosecond transillumination optical coherence tomography," Opt. Lett. **18**(12), 950–952 (1993).
4. D. A. Boas, D. H. Brooks, E. L. Miller, C. A. DiMarzio, M. Kilmer, R. J. Gaudette, and Q. Zhang, "Imaging the body with diffuse optical tomography," Signal Process. **21**, 57–75 (2002).
5. J. Swartling, A. Bassi, C. D'Andrea, A. Pifferi, A. Torricelli, and R. Cubeddu, "Dynamic time-resolved diffuse spectroscopy based on supercontinuum light pulses," Appl. Opt. **44**(22), 4684–4692 (2005).
6. G. Kumar, and J. M. Schmitt, "Optimal probe geometry for near-infrared spectroscopy of biological tissue," Appl. Opt. **36**(10), 2286–2293 (1997).
7. F. E. W. Schmidt, M. E. Fry, E. M. C. Hillman, J. C. Hebden, and D. T. Delpy, "A 32-channel time-resolved instrument for medical optical tomography," Rev. Sci. Instrum. **71**(1), 256 (2000).
8. B. Pogue, M. Testorf, T. McBride, U. Osterberg, and K. Paulsen, "Instrumentation and design of a frequency-domain diffuse optical tomography imager for breast cancer detection," Opt. Express **1**(13), 391–403 (1997).
9. K. Chen, L. T. Perelman, Q. Zhang, R. R. Dasari, and M. S. Feld, "Optical computed tomography in a turbid medium using early arriving photons," J. Biomed. Opt. **5**(2), 144–154 (2000).
10. C. V. Zint, W. Uhring, M. Torregrossa, B. Cunin, and P. Poulet, "Streak camera: a multidetector for diffuse optical tomography," Appl. Opt. **42**(16), 3313–3320 (2003).
11. M. J. Yadlowsky, J. M. Schmitt, and R. F. Bonner, "Multiple scattering in optical coherence microscopy," Appl. Opt. **34**(25), 5699–5707 (1995).
12. A. Wax, and J. E. Thomas, "Measurement of smoothed Wigner phase-space distributions for small-angle scattering in a turbid medium," J. Opt. Soc. Am. A **15**(7), 1896–1908 (1998).
13. R. K. Wang, "Signal degradation by multiple scattering in optical coherence tomography of dense tissue: a Monte Carlo study towards optical clearing of biotissues," Phys. Med. Biol. **47**(13), 2281–2299 (2002).
14. S. Farsiu, J. Christofferson, B. Eriksson, P. Milanfar, B. Friedlander, A. Shakouri, and R. Nowak, "Statistical detection and imaging of objects hidden in turbid media using ballistic photons," Appl. Opt. **46**(23), 5805–5822 (2007).
15. J. W. Pyhtila, R. N. Graf, and A. Wax, "Determining nuclear morphology using an improved angle-resolved low coherence interferometry system," Opt. Express **11**(25), 3473–3484 (2003).
16. R. N. Graf, W. J. Brown, and A. Wax, "Parallel frequency-domain optical coherence tomography scatter-mode imaging of the hamster cheek pouch using a thermal light source," Opt. Lett. **33**(12), 1285–1287 (2008).

#141183 - $15.00 USD Received 18 Jan 2011; revised 14 Feb 2011; accepted 15 Feb 2011; published 17 Feb 2011

17. R. Splinter, R. H. Svenson, L. Littmann, J. R. Tuntelder, C. H. Chuang, G. P. Tatsis, and M. Thompson, "Optical properties of normal, diseased, and laser photocoagulated myocardium at the Nd: YAG wavelength," Lasers Surg. Med. **11**(2), 117–124 (1991).
18. R. Splinter, W. F. Cheong, M. J. van Gemert, and A. J. Welch, "In vitro optical properties of human and canine brain and urinary bladder tissues at 633 nm," Lasers Surg. Med. **9**(1), 37–41 (1989).
19. N. Valim, J. Brock, and M. Niedre, "Experimental measurement of time-dependant photon scatter for diffuse optical tomography," J. Biomed. Opt. **15**(6), 065006 (2010).
20. M. Burcin Unlu, O. Birgul, R. Shafiiha, G. Gulsen, and O. Nalcioglu, "Diffuse optical tomographic reconstruction using multifrequency data," J. Biomed. Opt. **11**(5), 054008 (2006).

1. Introduction

Optical imaging is an attractive means of assessing tissue health and structure. Unfortunately at optical frequencies, imaging within tissue is limited by a strong scattering characteristic that attenuates the incident illumination and obscures the desired signal beneath a diffusely scattered background. Numerous optical techniques have been developed to image in the presence of scattering, including confocal microscopy and optical coherence tomography (OCT). These techniques extend the range of imaging in tissues to a millimeter or more by rejecting out of focus light and improving sensitivity.

In contrast to the 1-2 mean free scatting paths typical for confocal microscopy, OCT can image through approximately 27 mean free scattering paths (approximately 1-2 mm in soft tissue) by exploiting interferometric detection and low coherence light sources. Coherence gating in OCT enables shot noise limited detection while excluding photons that have not traveled a given optical path length (OPL) [1,2]. Under the assumption that few photons scatter more than once, each path length measurement is converted into a depth resolved profile using knowledge of the medium refractive index. Unfortunately, while OCT can reject ballistic photons by comparing their path length within the medium to that of a reference arm, it cannot reject photons that have accumulated a longer time of flight within a superficial depth by scattering multiple times [3]. Thus as the number of mean free scattering lengths into a sample increases, the ballistic signal is reduced through attenuation while the background of multiple scattered photons increases. Eventually, either shot noise or multiply scattered photons overwhelm the ballistic signal and deeper imaging is no longer possible, imposing a practical depth limit on coherence gated imaging in OCT.

As an alternative, a complementary set of techniques based on diffuse photon path lengths exploit this multiply scattered light to achieve deeper imaging. In diffuse optical tomography (DOT) techniques, illumination and collection are arranged with the goal of recovering target information using primarily multiply scattered light and tomographic inversion algorithms. Because the absorption of typical tissues is low compared to the scattering coefficient, photons can pass through many scattering events before being absorbed, potentially allowing absorption information to be obtained for tissue depths well beyond the ballistic limit [4]. Several strategies exist for recording diffuse light and recovering an image. Most involve spectrally resolving the diffuse light to examine scattering or absorption variations with wavelength [5], spatially resolving the collection and illumination points in order to infer probable photon paths from the system geometry [6], or temporally resolving photons in order to measure optical path length [7]. The spatial distribution or spectral properties of scatterers or absorbers within the medium is then estimated from temporal, spectral or spatial information using an inversion model.

Conceptually time-resolved diffuse optical tomography (TR-DOT) is performed similarly to OCT; photons are compared against an electronic reference signal, versus an optical reference signal in OCT, and then binned by time interval. The comparison can be performed in the frequency domain, in which case waves of photons are modulated at frequencies of a few hundred MHz, and the phase delay and attenuation due to passage through tissue is measured [8]. This method has good throughput, but poor time resolution owing to the relatively low modulation speeds that are possible in tissue. Alternatively, measurements can be performed in the time domain by directly comparing pulsed laser light to a electrical

#141183 - $15.00 USD Received 18 Jan 2011; revised 14 Feb 2011; accepted 15 Feb 2011; published 17 Feb 2011

reference signal using a streak camera [9,10] or a time correlated single photon counter (TCSPC) [7]. Both of these techniques suffer from high cost, require complicated electronics and have low throughput. In TCSPC, the most common method, photons are binned one at a time at rates in the tens of MHz.

In OCT, low coherence interferometry is used to gate signal detection instead of an electronic reference. Incoming photons are interferometrically detected by the overlapped reference field, which serves to enhance signal strength. The time resolved data is separated into temporal bins, and the optical energy per temporal bin is detected. This approach has an enormous advantage in throughput because individual photons do not need to be counted. For example in a typical time domain OCT system operating in the NIR, the maximum number of photons that are detected per second is on the order of 10^{15}. In comparison, commercial high speed TCSPCs have an acquisition rate on the order of 10^{6} photons per second, approximately 9 orders of magnitude less. By exploiting the extremely high throughput and shot noise limited sensitivity of low coherence interferometry, it has been possible to construct imaging systems operating at extremely high speeds without sacrificing image contrast or axial resolution [2].

The possibility of using interferometry to measure multiply scattered light was addressed early on during the development of OCT by Hee et al. who performed time resolved transmission measurements of scattering media showing photons traversing 50 mean free paths (MFPs) [3]. Later experiments by Yadlowsky et al. demonstrated detection of multiply scattered photons in reflection mode [11]. Wax and Thomas built on this work by using the Wigner distribution to show that forward scattered light carries structural information within its angular distribution even after multiple scattering, whereas diffuse light does not carry structural information nor have a well defined angular distribution [12]. Subsequently Wang performed detailed Monte Carlo simulations of diffuse imaging in conventional OCT system aimed at exploring the loss of contrast in ballistic imaging; however these simulations revealed that multiply scattered photons received from well beyond the ballistic limit still carried substantial structural information [13]. Finally, Farisu et al. considered the resolution of multiply scattered and ballistic imaging systems from a statistical detection standpoint, and showed using arguments based on a maximum likelihood estimator that optimal detection of scatterers embedded in turbid media required considering both ballistic and multiply scattered photons [14]. These previous results suggest that using multiply scattered low coherence interferometry (MS/LCI) may be an attractive alternative to traditional diffuse imaging modalities by allowing high throughput time-resolved measurements.

To explore the feasibility of MS/LCI, we employ a time-domain low coherence interferometry system operating in reflection mode which provides distinct illumination and collection pathways. This system incorporates angle resolved collection as well as a variable illumination angle in order to optimize the ability of the system to collect photons with structural information. Using this system we confirm that multiply scattered photons can be readily detected interferometrically, even after many scattering events, and then use this approach to demonstrate OCT imaging well beyond the ballistic limit.

2. Experimental setup

In the experimental system [Fig. 1(a)], light from a mode-locked titanium sapphire laser at 830 nm with a coherence length of 30 μm is separated into sample (blue) and reference (red) arms. A pair of acousto-optic modulators at 110 and 120 MHz respectively generate a net frequency shift of 10MHz between the arms. On the sample arm, mirror M1 allows adjustment of the illumination angle by lateral translation, while lens L1 can be translated off-axis to adjust the collection angle using an approach developed previously for angle resolved low coherence interferometry [15]. On the reference arm, a mechanically translated retro-reflector RR is used to vary the path length. Finally, a stepper motor is used to laterally translate the sample to execute B mode scans. Detection is performed by a balanced

#141183 - $15.00 USD Received 18 Jan 2011; revised 14 Feb 2011; accepted 15 Feb 2011; published 17 Feb 2011

photodiode receiver (NewFocus Model 1807). In contrast to conventional OCT, light scattered from the sample is not focused onto the detector, but is caused to diverge by lens L3 such that only the angular component selected to be parallel to the reference arm is detected. After photodetection, the 10MHz beat signal is demodulated by an Agilent E4411B spectrum analyzer, and the output is squared and detected by an SRS530 lock-in amplifier to further suppress out of band noise.

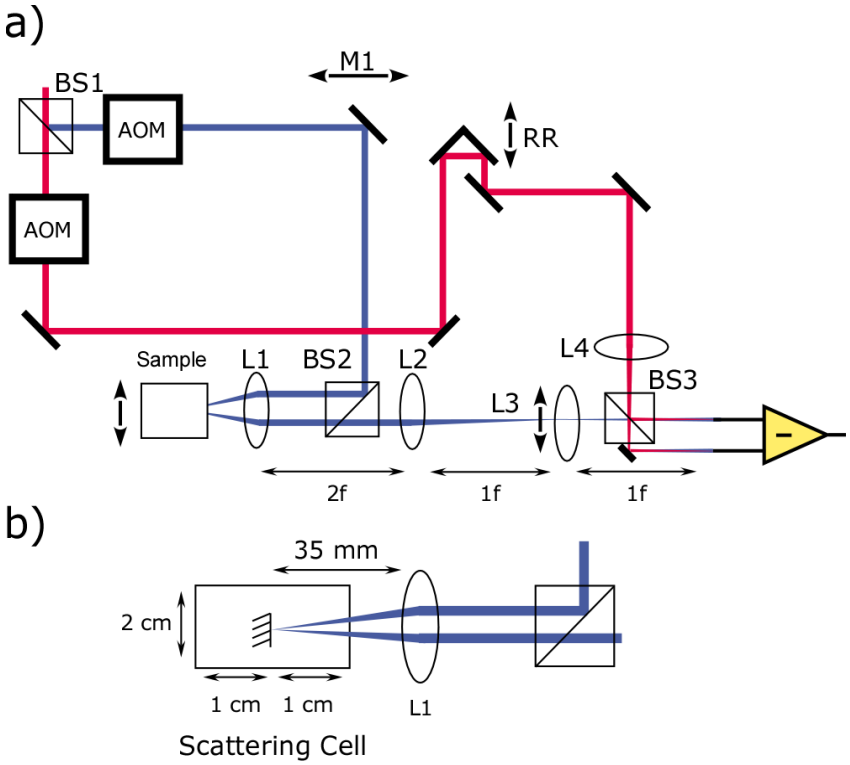

Fig. 1. Schematic of the time domain MS/LCI system. a) 830 nm Ti:Saphire light is divided into sample (blue) and reference (red) arm paths. A pair of acousto-optic modulators (AOMs) frequency shift the sample and reference arms such that a 10MHz frequency offset exists between them. Mirror M1 adjusts the illumination angle onto the sample, while lens L3 (f = 100 mm) adjusts the collection angle. A retro-reflecting prism (RR) is used to perform depth scans, while B scans are performed by translating the entire sample enclosure. L1 (f = 35 mm) and L2 (f = 100 mm) form a 4f relay onto the center of L4 which can be translated to adjust the collection angle. b) Close up of the sample chamber. A 4 mm gold coated reflector is suspended in the middle of a 2x2 cm box filled with scattering media.

The combination of lock-in detection and time-domain acquisition allows for very narrow detection bandwidths and long scan depths. These capabilities are challenging for frequency domain detection which requires very high spectral resolution to measure long path lengths but would then demand longer integration times [2]. The use of time-domain acquisition is advantageous for studying scattered light because photons are summed incoherently when the power spectrum is detected compared to the coherent detection in frequency domain detection, and thus time-domain avoids the need to remain phase stable over long integration times [16]. The SNR of the system was experimentally demonstrated to be 151dB and the maximum scan distance was 50 mm (equivalent to 450 ps in media). This exceeds the SNR of conventional Fourier domain OCT (FD-OCT) systems, and allows extremely long depth scans, but requires long scan times of approximately 1 minute per 1 mm of A-scan depth.

Imaging experiments were performed using a 2 cm by 2 cm by 1 cm chamber with a target consisting of a gold coated coverslip 3.3 mm wide suspended 1 cm from the front and side

#141183 - $15.00 USD Received 18 Jan 2011; revised 14 Feb 2011; accepted 15 Feb 2011; published 17 Feb 2011

surfaces [Fig. 1(b)]. The dimensions were chosen to be large enough that interaction with the walls would not significantly influence the scattered field over the range of time of flights recorded. The chamber was filled with solutions of either 1 μm or 11 μm polystyrene microspheres (n = 1.59) suspended in 20% polyethylene glycol (PEG) for increased viscosity (n = 1.34). The illumination angle was set to 6 degrees and was chosen to ensure that light which was multiply scattered at depths superficial to the target would have a decreased probability of reaching the collection optics. Each imaging scan was performed over a 10 mm axial and 7 mm lateral range using 9 mW of illumination power. Individual A-scans were processed to remove the diffuse background by fitting an exponential to the decay of the ballistic signal and then subtracting. This step is equivalent to logarithmic amplification and is essential for separating weak diffuse signals from overlaying background scattered light. The optical properties of the scattering media were calculated using Mie theory from the manufacturer's specifications and the measured media refractive index. For 1 μm beads, the scattering coefficient was calculated to be 230 1/mm with an anisotropy coefficient (g) of 0.95 using Mie theory. For 11 μm bead solution the scattering coefficient was calculated to be 26.7 1/mm and the anisotropy coefficient 0.985. For anisotropic media, the reduced scattering coefficient $\mu_s' = \mu_s(1-g)$ which takes into account that forward scattered light retains its directionality is often used. Reduced scattering coefficients of 9.2 and 0.261 1/mm respectively were computed for the stock solutions. The solutions were then diluted down to produce the desired total ballistic scattering rates for the imaging experiments. It should be noted that the anisotropy values are deliberately large to simplify experimental measurements, but are actually comparable to or below reported values for several human tissues, including myocardium, fat, and brain tissue [17,18].

3. Results

3.1 1 μm bead solution

Samples of 1 μm bead solution were prepared with increasing concentration and tomographically imaged with illumination and collection optics fixed at 6 degrees above and below the normal incidence respectively. Concentrations were chosen to begin with 20 mfp for the 1 cm path length the target, close to the ballistic limit, and then extend towards increasing scattering until imaging was no longer possible [Fig. 2]. Beginning with 20 mfp, both the ballistic and diffuse signals are apparent with nearly equal peak amplitude but separated by 600 μm of OPL or a time of flight of 2.7 ps. With increasing scatterer concentration, several trends are apparent in imaging the target. First, multiple scattering rapidly broadens the tight ballistic peak until by 35 mfp (equivalent to 1.75 transport mean free paths) it spans the entire 4 mm of imaged OPL. Additionally, in contrast to the temporal profile, the lateral profile spreads out more slowly due to the anisotropic propagation in the media.

#141183 - $15.00 USD Received 18 Jan 2011; revised 14 Feb 2011; accepted 15 Feb 2011; published 17 Feb 2011

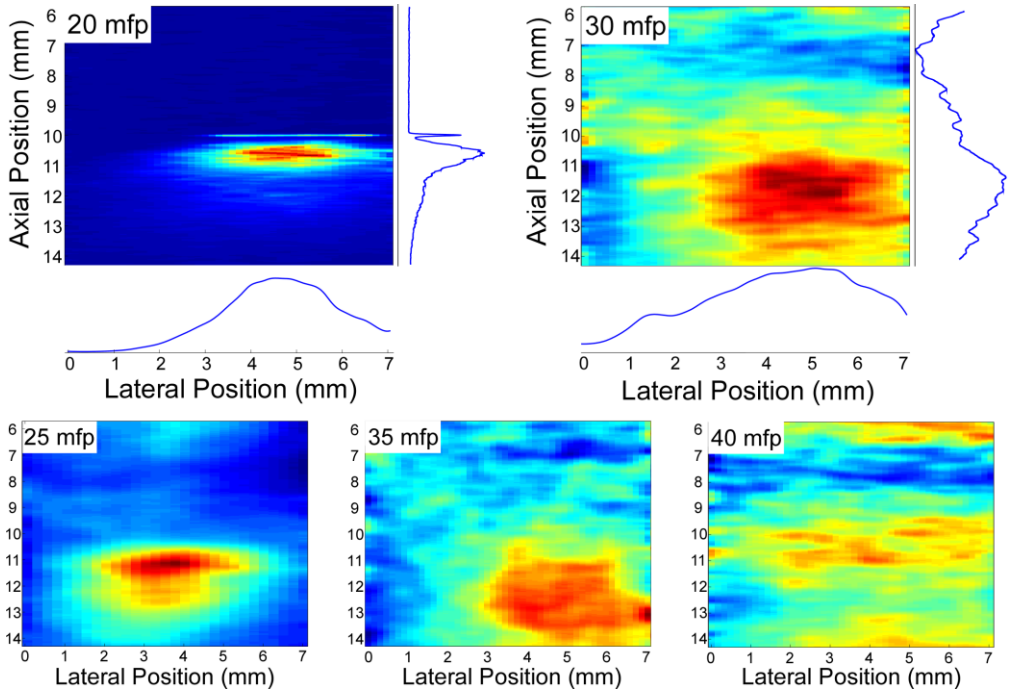

Fig. 2. Tomographic images of a 3.3 mm wide test reflector located 10 mm beneath the surface of 1 μm microsphere scattering media for increasing concentrations, corresponding to 20, 25, 30, 35, and 40 mfp. Contrast gradually decreases until at 40 mfp the object is obscured. The 20 and 30 mfp scans have axial and lateral profiles shown through the center of the reflector, highlighting the axial and lateral extent of the diffusely scattered signal. Note that the 20 mfp image has both ballistic and diffuse peaks.

3.2 Comparison to ballistic imaging

Figure 3 shows enlarged axial and transverse scans for ballistic light and diffuse light after 20 and 30 mfp. As in conventional OCT, the ballistic peak has an axial resolution comparable to the coherence length, 34 μm experimental vs. 30 μm theoretical 10 to 90% rising width, with the difference due to dispersion in the media. In contrast, the rising edge of the diffuse peak extends 440 μm at 25 mfp and 870 μm at 30 mfp. The lateral resolution is similarly degraded, increasing from a nearly diffraction limited 35 μm 10 to 90% width for the ballistic peak, up to 2.3 mm and 3.0 mm for 25 and 30 mfp diffuse imaging.

#141183 - $15.00 USD Received 18 Jan 2011; revised 14 Feb 2011; accepted 15 Feb 2011; published 17 Feb 2011

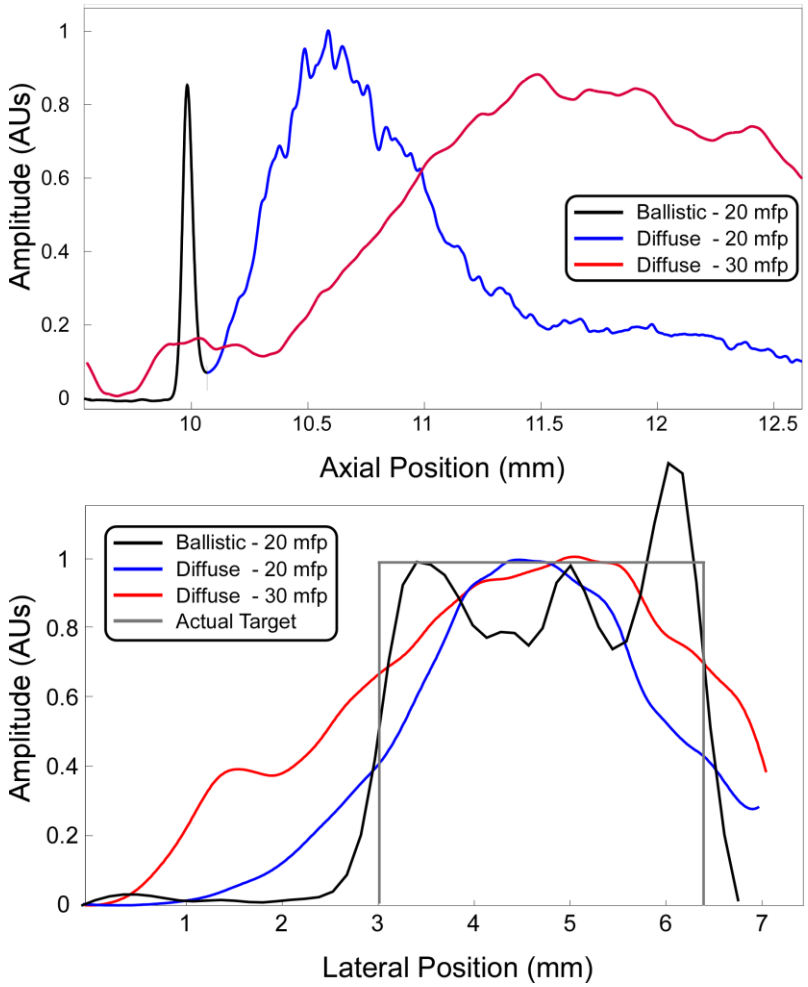

Fig. 3. Axial (top) and lateral (bottom) resolution comparison for the 20 mfp ballistic (black), 20 mfp diffuse (blue) and 30 mfp diffuse (red) imaging experiments.

3.3 11 μm bead Solution

The knife-edge experiments were repeated using 11 μm bead solutions to explore forward scattering in highly anisotropic media (Fig. 4). Initial scans were performed at 50 mfp and revealed a clearly defined diffuse peak with no ballistic contribution. Concentration was increased to 94 mfp (equivalent to 1.4 transport mean free paths) where the diffuse signal dropped to nearly the level of the diffuse background. As with the 1 μm bead solutions, lateral and axial resolution steady degraded with increasing number of scattering events.

#141183 - $15.00 USD Received 18 Jan 2011; revised 14 Feb 2011; accepted 15 Feb 2011; published 17 Feb 2011

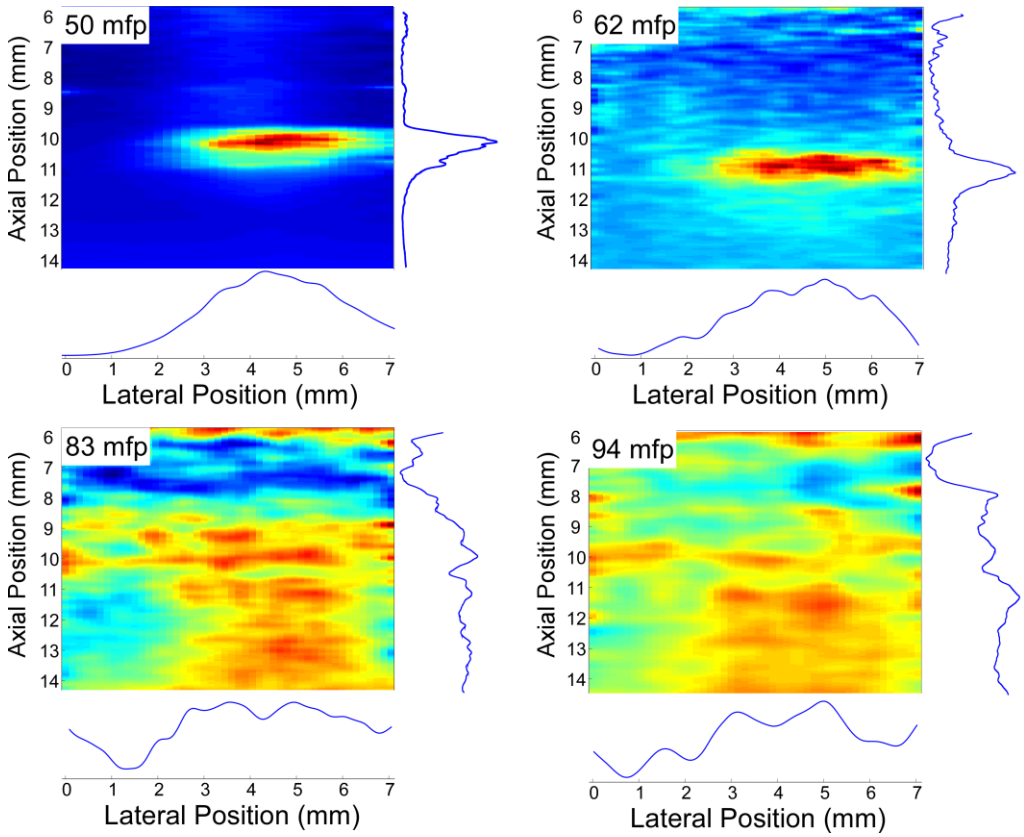

Fig. 4. Tomographic images of a 3.3 mm wide test reflector located 10 mm beneath the surface of 11 μm microsphere scattering media for increasing concentrations, corresponding to 50 mfp, 62 mfp, 83 mfp and 94 mfp. With increasing scattering the reflector signal broadens out in both time and lateral position, resulting in progressively decreased resolution. However, even at 94 mfp photons that have interacted with the reflector remain distinct from the diffuse background signal.

3.4 Attenuation of multiply scattered light

Transport theory predicts that diffusely scattered photons are exponentially attenuated with increasing number of mean free paths traversed, but at a reduced rate compared to ballistic photons because the transport mean free path is longer than the ballistic mean free path. This effect was confirmed in Fig. 5 by plotting the peak reflector intensity versus turbidity for each of the scattering solutions. The effective attenuation coefficient in the diffuse regime was found to be intermediate between the ballistic and transport scattering coefficients. For example, using an anisotropy value of 0.96 for 1 μm beads, the transport attenuation coefficient is calculated to be 25 times less than the ballistic coefficient. However, the transport regime attenuation seen in Fig. 5 is only 4.1 times less than the predicted exponential attenuation for ballistic light.

#141183 - $15.00 USD Received 18 Jan 2011; revised 14 Feb 2011; accepted 15 Feb 2011; published 17 Feb 2011

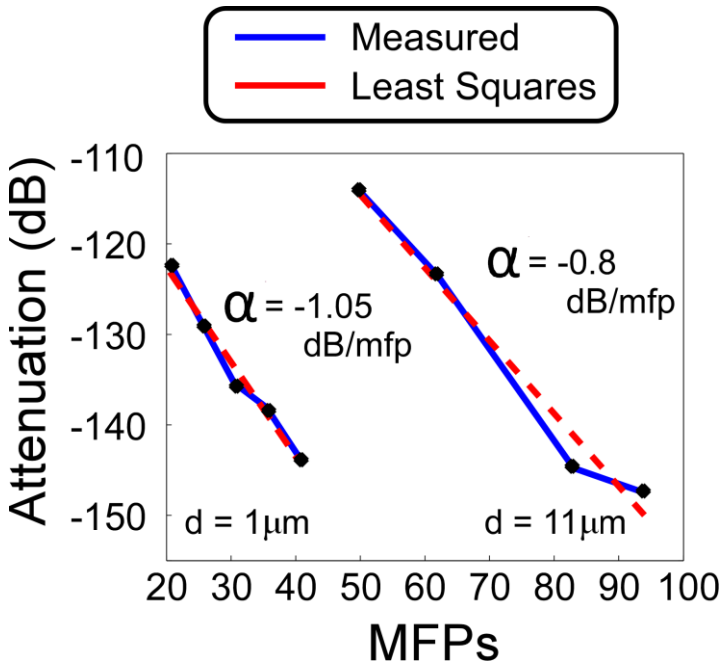

Fig. 5. Detected power relative to illumination power for both bead sizes as a function of mean free paths into the scattering media. Least squares fits to the attenuation verses mean free scattering events yield attenuation coefficients for multiply scattered photons of –1.05 and –0.8 dB/mfp for 1 and 11 μm microspheres respectively, significantly less than the 4.34 dB/mfp for ballistic attenuation.

3.5 Resolution

Figure 6 shows the achieved imaging resolution in both the axial and lateral dimensions, taken as the 10 to 90% rise from each B-scan image. For the shortest number of mean free paths, lateral resolution is highest, but quickly saturates at a maximum value. Beyond 30 mfp, the lateral resolution no longer exhibits a statistically significant increase. This likely reflects the transition from ballistic imaging below 30 mfp where most photons are minimally scattered to propagation via multiple small angle scattering. In this regime, additional broadening in the lateral direction is counterbalanced by increased optical path length, resulting in rejection by coherence gating. In contrast, axial resolution is steadily degraded with increasing number of mean free paths as additional scattering events randomly contribute to the optical path length of each photon.

#141183 - $15.00 USD Received 18 Jan 2011; revised 14 Feb 2011; accepted 15 Feb 2011; published 17 Feb 2011

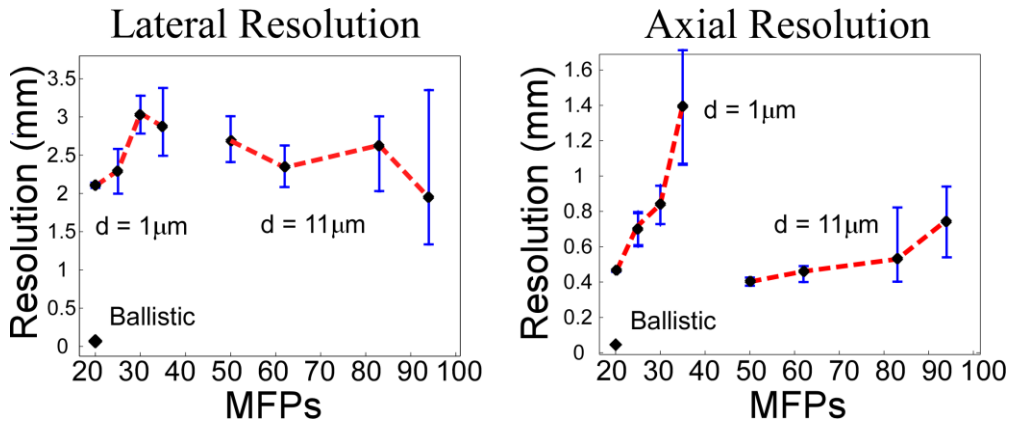

Fig. 6. Lateral and axial resolution plots for imaging through samples of 1 and 11 μm beads of various concentrations, given by mean free path (mfp). Resolution was defined as the 10 to 90% rise in each dimension. Error bars are computed from the standard deviation of the background signal immediately adjacent to the reflector surface. Lateral resolution is relatively insensitive to number of scattering events, while axial resolution degrades continuously with increasing scattering.

4. Discussion

The combination of multiply scattered light, angle resolved collection, and separate illumination and collection pathways allow extended imaging depth in highly scattering media over conventional approaches such as confocal microscopy or OCT. In the latter two methods, imaging deeper into a scattering sample produces an exponential decay of the signal as photons are lost due to scattering events. This restricts these approaches from operating beyond the ballistic limit [1], but this imaging simplifies interpretation of signals because each photon can be assumed to have scattered only a single time. In contrast, MS/LCI employs multiple forward scatter to increase imaging depth. Thus, photons are only lost when they scatters outside of the forward scattering cone, either through a single large angle scattering, or after multiple forward scattering events that cumulatively alter its direction. This results in a much lower effective scattering coefficient because only a fraction of scattering events actually attenuate the beam [12].

The attenuation coefficients measured in the multiply scattered regime (Fig. 5) indicate that 76% and 82% of scattering events for 1 μm and 11 μm respectively preserve photons within the forward scattering cone. These results agree with the Mie scattering pattern for 1 μm and 11 μm beads, which are highly peaked in the forward direction, such that the majority of scattering events deviate from the forward direction by less than a few degrees. The difference between the attenuation measured using MS/LCI and the mean free transport length predicted using transport theory can also be reconciled using these arguments. The mean free transport length is the product of the anisotropy coefficient, defined as the average of the cosine of the scattering angle, and the scattering mean free path. The mean free transport length assumes that photons scattering at larger angles will also contribute to the light transport. However, photons scattering at larger angles do not contribute here since they travel longer distances, and thus they are effectively lost because they do not arrive in time to contribute to the same coherence gated temporal bin as photons in the forward scattered cone. Because the mean free transport length does not account for time resolved detection, it does not provide a good model here as it significantly underestimates the actual attenuation.

The distinct illumination and collection pathways combined with angle resolved collection are essential to the MS/LCI technique because they effectively allow triangulated detection of multiply scattered photons which leads to further rejection of diffusely scattered light in favor of forward scattered photons. The advantage of this geometry is apparent when considering

#141183 - $15.00 USD Received 18 Jan 2011; revised 14 Feb 2011; accepted 15 Feb 2011; published 17 Feb 2011

the possible paths of each path length matched photon; either propagating to the focal plane of the lens, scattering several times, and then eventually passing into the collection optics or else scattering multiple times superficial to the focal plane and eventually returning to the collection beam path with the correct path length and angle. Because the range of collected angles is restricted to be relatively narrow, few photons will scatter into the collection beam path without passing through the focal plane. The effects of coherence gating and the triangulation scheme are therefore complementary; the former rejecting superficially scattered photons while providing time of flight information, the latter rejecting diffuse light originating away from the sample plane.

The combination of imaging using forward scattered light and triangulation results in distinct collection regions relative to focal plane of the lens. Superficial to the focal plane of the lens, few photons are collected because the illumination and collection beams do not intersect. At the focal plane of the lens, the two beams intersect and sensitivity is maximized. Below the focal plane, the beams no longer overlap, so sensitivity is decreased. However, a large number of photons originating in the focal plane undergo multiple scattering events, and therefore accumulate longer path lengths that would indicate that the detected signal arises from below the focal plane of the lens. This effect is apparent in Fig. 3 at 30 mfp, where nearly all backscattering takes place at the target located in the focal plane, but the majority of the photons appear to originate from deeper in the sample. MS/LCI images are therefore the superposition of two different effects: time resolved interferometry that detects photons based on their time of flight, and a time insensitive triangulation that rejects photons based on physical depth into the media. Although not widely used in OCT or confocal microscopy, such triangulation schemes have been used in diffuse tomography to reject background diffuse light or enhance contrast [6,8].

The MS/LCI technique presented here of using low coherence interferometry to image with multiply scattered light offers both advantages and disadvantages over conventional OCT. The primary disadvantage is that the resolution of multiply scattered imaging does not approach either the coherence gated axial resolution or the confocal lateral resolution of conventional OCT. Even at an equal number of scattering path lengths into the media, the ballistic signal is shown to be at least an order of magnitude greater resolution both laterally and axially. The primary advantage however, is that as imaging depth increases, the contrast of the tomographic images decreases much more slowly than in OCT due to the lower effective scattering coefficient achieved in this geometry. In highly anisotropic media, we have demonstrated more than 3 times the maximum penetration possible with ballistic imaging techniques such as OCT.

MS/LCI has a number of advantages compared to conventional time-resolved DOT, techniques. Principally, interferometry allows an extremely large detection throughput combined with high dynamic range at reasonable cost, which is generally not possible with TCSPC or streak cameras based on direct detection. Additionally, temporal resolution is limited only by the temporal coherence of the source and not the detection electronics; for superluminescent diodes (SLDs) this is tens of microns OPL, significantly better than existing methods. To understand the advantages of MS/LCI, it is helpful to consider the capabilities of current time resolved photon detection methods. Time domain systems provide good time resolution and sensitivity (typically on the order of 100 picoseconds and shot noise limited [5,19]) but sacrifice throughput and dynamic range while requiring expensive detectors. Frequency domain DOT systems have high throughput and low cost but relatively poor temporal resolution and reduced sensitivity at short time scales [19,20]. In contrast, LCI can simultaneously provide approximately 3 orders of magnitude superior time resolution to time domain methods, and superior throughput and dynamic range to frequency domain methods at a reasonable cost. Taken together, these advantages provide the potential for increased imaging speed and improved contrast compared with existing techniques.

#141183 - $15.00 USD Received 18 Jan 2011; revised 14 Feb 2011; accepted 15 Feb 2011; published 17 Feb 2011

5. Conclusion

We have demonstrated the feasibility of tomographic imaging by using low coherence interferometry for time-resolved measurement of multiply-scattered light. The resolution and imaging depth were characterized for the presented imaging system based on this principle. By exploiting the time resolution and sensitivity of the approach, and the ability to employ photons propagating by multiple scattering, we have provided proof of concept tomographic imaging through nearly 100 scattering lengths, significantly exceeding the ballistic imaging limit.

Acknowledgments

This work was supported by the US Air Force Research Laboratory under contract #FA8650-09-C-7932 and the National Institute of Health under grant R01CA138594. The views expressed are those of the author and do not reflect the official policy or position of the Department of Defense or the U.S. Government. Approved for Public Release, Distribution Unlimited.

#141183 - $15.00 USD Received 18 Jan 2011; revised 14 Feb 2011; accepted 15 Feb 2011; published 17 Feb 2011